Interaction between counter-rotating azimuthal and axial liquid metal flows in cylindrical channel

Ilya Kolesnichenko [*] and Vladimir Ozernykh [†]
Institute of Continuous Media Mechanics UB RAS, Perm, Russian Federation

(Received 13 July 2025; accepted 30 October 2025; published 20 November 2025)

The mechanism of generation of a localized solitary azimuthal vortex in an axial liquid metal flow is found by numerical simulations. Initially, two counter-rotating magnetic field inducers create two vortices by electromagnetic forces in the cylindrical channel with an axial through flow of liquid metal. Beyond a certain threshold of azimuthal forcing, the second vortex is completely suppressed by the first counter-rotating vortex. The threshold value is reached when the Reynolds numbers for rotating and axial flows become equal. The solitary vortex has clear-cut boundaries. After the switch-off the driving forces, the solitary vortex is frozen in the axial flow when transferred by it.

DOI: 10.1103/7bs3-xt8t

I. INTRODUCTION

Vortex and helical flows of electrically conductive media in cylindrical channels are extensively studied in Magnetohydrodynamics (MHD) [1]. These flows are of interest from both the fundamental and applied point of view. For instance, in fundamental research, helical flows of liquid metal in a cylindrical channel are a subject of intensive theoretical and experimental study of the MHD-dynamo effect [2]. In these studies, the swirl flows are generated either by a rotating propeller [3] or a stationary divertor or screw [4].

It is well known that vortical and helical flows of liquid metal in a cylindrical channel can be created in a noncontact way. This makes it possible to exclude additional devices and parts from the cylindrical tube. Such flows are driven by electromagnetic forces induced by rotating and traveling magnetic fields (RMF and TMF) [5], which are generated by external inductors located outside the channel. Such flows are widely studied in applications related to electromagnetic stirring of melt during its crystallization [6,7]. Thus, MHD methods provide the easy and most convenient way of noncontact generation of strong helical flows in liquid metals.

They can be used to create not only a continuous swirl of a through flow, but also a short-time one. This results in the appearance of spatially localized vortex, which will migrate together with the flow. By tracking the vortex motion using, again, the electromagnetic methods, the velocity of the axial transit flow can be evaluated. The problem, however, is that because of traditional use of RMF, in this case, the vortex will not have distinct boundaries. There is a simple method that allows the formation of the vortex with clear-cut boundaries. This can be done by using two or more sequentially located RMF inductors, which provide alternation of rotational directions, as described in Ref. [8]. The study for a pair of vortices has shown [9] that the boundary between the vortices is indeed localized in space. However, thus far the behavior of such a pair of vortices in the axial through flow in the channel is not clearly understood, which is the problem investigated in this paper.

There are a large number of electromagnetic techniques for measuring the velocity and flow rate of liquid metal [10–13]. The emphasis is placed on studying the processes in conductive

[*]Contact author: kiv@icmm.ru
[†]Contact author: ozernykh.v@icmm.ru

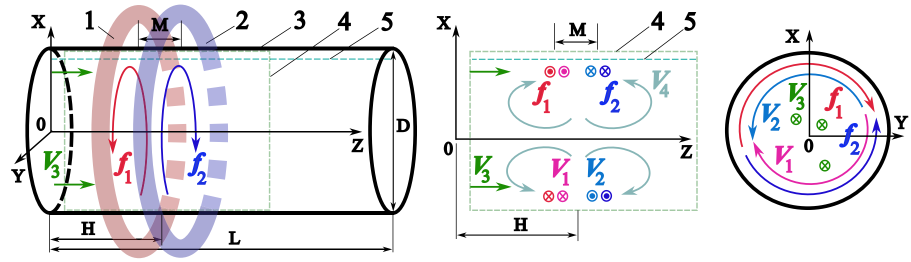

FIG. 1. Schematic of the channel and flows in spatial, cross-sectional, and axial views: 1, 2: inductors of RMF; 3: channel; 4: axial cross section; and 5: line segment for plotting the results.

[14,15], inductive [16–18], and Lorentz-force [19,20] flowmeters. A common disadvantage of these techniques is the need to calibrate them using circuits with a relevant flowmeter. The correlation method, which is one of the most reliable ways of measuring the velocity and flow rate of liquid metal, is devoid of this disadvantage. It is based on correlation analysis of some random fluctuations in velocity or temperature of the flow [21]. Actually, it measures the time it takes for the flow to move some measurable tracer (marker) from one sensor to another, or, in the other words, it measures the displacement of a marked Lagrangian liquid particle.

One of the ways to create a localized vortex in the flow is the magnetic obstacle [22]. This method consists in generating a localized electromagnetic force and, as a consequence, small-scale velocity pulsations when liquid metal flows through a permanent, spatially localized magnetic field, which is perpendicular to the flow. The study shows that this technique can be used to measure the velocity of transit flow based on the correlation analysis of temperature pulsations [23]. The disadvantage of these techniques is the small region of the flow for measuring the pulsations, which requires consideration of velocity profile to determine the flow rate. This accounts for the relevance of the problem of large-scale velocity pulsations generated in the axial through flow of liquid metal and localized in the direction of the channel axis.

This paper investigates the behavior of vortex flow, which is produced in a cylindrical channel 3 by counter-rotating MF sources 1 and 2 (Fig. 1). The RMFs produce electromagnetic forces that have azimuthal components f_1 and f_2 and less intense radial components. These forces create primary azimuthal rotating flows V_1 and V_2. In the channel, there is also an axial flows V_3 initiated by an external source. It is shown in Ref. [9] that this pair of azimuthal vortices V_1 and V_2 gives rise to a pair of secondary poloidal vortices V_4. The velocity V_4 is considerably smaller than V_1, V_2, and V_3. The electromagnetic forces begin to act on the existing stationary flow traveling with the velocity V_3 at a specified time t_1. The action of the applied forces on the liquid metal lasts for a prescribed time period $\Delta t = t_2 - t_1$ and is switched out at time t_2.

Then, based on the numerical simulation, we model a stationary through-flow regime in the absence of o electromagnetic forces. This regime is taken as the initial state for calculations, which are performed with consideration of electromagnetic forces.

The objective of this study is to investigate the behavior of the generated vortex both during its evolution and during its migration along the flow direction. The major interest is in getting answers to the following two questions. Is it possible to create a spatially localized vortex against an axial transit flow? How far can this vortex be carried by the transit flow without significant change? To answer these questions, we have carried out a numerical investigation using mathematical modeling and correlation analysis.

II. MATHEMATICAL MODEL

The mathematical model is based on the MHD equations describing the interaction of electric and magnetic fields with moving electrically conductive media [1]. One equation describes the transport of a magnetic field by a moving electrically conductive fluid. The other two equations are the Navier-Stokes equation, containing the term of electromagnetic force, and the continuity equation.

The reduced formulation the mathematical model equations in the frame of electrodynamics approach is based on the following estimates. The intensity of magnetic field transfer by a moving electrically conductive medium is characterized by the dimensionless magnetic Reynolds number $\mathrm{Re}_m = U\delta\sigma\mu_0 = 0.02\ldots0.28$, where U is the characteristic velocity of the medium, $\delta = 0.029m$ is the value of the skin layer, determined by the depth of penetration of the magnetic field into the liquid metal [24], σ is the electrical conductivity of the medium, and μ_0 is the magnetic constant. Preliminary estimates have shown that $\mathrm{Re}_m \ll 1$ for the values reached in this study. This means that the magnetic field transport by the flow of the electrically conductive fluid can be neglected. In turn, the strength of the braking effect of an external magnetic field on the flow of an electrically conductive fluid is described by the dimensionless Hartmann number $\mathrm{Ha} = B_0\delta\sqrt{\sigma/\eta} \sim 1$, where B_0 is the characteristic value of magnetic induction, η is the dynamic viscosity of the fluid. Preliminary estimates have shown that $\mathrm{Ha} \ll 10$ for the values achieved in this study. This implies that the magnetic field has no significant braking effect on the flow [1,10,25]. Thus, in this proposed formulation of the problem, the interaction between the magnetic field and the flow of the conductive fluid can also be neglected. This allows us to divide the model into two parts: electrodynamic and hydrodynamic, and to develop separately their mathematical formulations. Thus, the electrodynamic part of the mathematical model is based on Maxwell's equations:

$$\nabla \times \vec{H} = \vec{j}; \tag{1}$$

$$\nabla \times \vec{E} = -\frac{\partial \vec{B}}{\partial t}; \tag{2}$$

$$\nabla \cdot \vec{B} = 0; \tag{3}$$

$$\nabla \cdot \vec{E} = 0. \tag{4}$$

In these equations, Ampere's law (1) without taking into account displacement current describes the generation of magnetic field by the current. In equation (1), $\vec{j}$ is the density of alternating current passing through the conducting media, $\vec{H}$ is the strength of the alternating magnetic field generated by the alternating current.

The current density varies in time, executing harmonic oscillations with frequency f. The action of the magnetic field on volumes with media having different values of magnetic permeability μ results in their magnetization. In our study, for ferromagnets $\mu = 3 \times 10^3$, and for nonferromagnets it is assumed that $\mu = 1$. It is taken into account in the relationship between the magnetic induction and magnetic field strength $\vec{B} = \mu\mu_0\vec{H}$.

The alternating magnetic field, in turn, generates a vortex electric field $\vec{E}$, which is described by the electromagnetic induction equation (2). The resulting magnetic and electric fields are solenoidal, which follows from the Eqs. (3) and (4). This electric field is the electromotive force, whose action generates an eddy electric current in an electrically conductive medium. In the problem, there is no sense to take into account the induction of electric current by an alternating field in ferromagnetic laminated inductor elements and windings. Therefore, their electrical conductivity was assumed to be zero.

Under the action of an electric field, an electric current is generated in the conductive medium. In liquid-metal volume, this process is described by Ohm's law (5):

$$\vec{j} = \sigma\vec{E}, \tag{5}$$

with continuity condition for the electric current density (6):

$$\nabla \cdot j = 0. \tag{6}$$

The presence of electric current and magnetic field in an electrically conductive medium leads to the appearance of the net electromagnetic force (7), which should be reasonably taken into account only in liquid metal

$$\vec{f}^{\mathrm{em}} = \vec{j} \times \vec{B}. \tag{7}$$

The normal component of the electric current density is set to zero at the boundary of the liquid metal. The standard boundary conditions for magnetic induction are set at the boundaries between regions containing media with different values of magnetic permeability.

The standard boundary conditions are as follows. Since the channel wall is not taken into account in the calculations, at the boundaries of the liquid-metal region the current density is subject to the condition of zero normal component. At the interface between the media, the normal component of the electric field intensity undergoes a discontinuous jump, but the tangential component does not change. Similar effect is observed in the magnetic field. At the interface between two media, the normal component of the magnetic field intensity undergoes a sudden jump, while the tangential component does not change.

The flow of an electrically conducting medium in the electrodynamic approximation is described by the Navier-Stokes equation taking into account the action of the electromagnetic force (8), as well as by the continuity equation (9):

$$\frac{\partial \vec{V}}{\partial t} + (\vec{V} \cdot \nabla)\vec{V} = -\frac{\nabla p}{\rho} + \nabla \cdot [(\nu + \nu_t)(\nabla \vec{V} + \vec{V}\nabla)] + \frac{\vec{f}^{\mathrm{em}}}{\rho}, \tag{8}$$

$$\nabla \cdot \vec{V} = 0. \tag{9}$$

Here, ν is the molecular viscosity, ν_t is the turbulent viscosity, and ρ is the density of the liquid metal. At the side boundaries of the channel, the no-slip condition is prescribed. A turbulent velocity profile with a mean value V_T is used at the inlet boundary of the region. The length of the inlet section and the profile pattern do not play a significant role in this problem, because the electromagnetic force strongly disturbs the flow structure. Indeed, the entry of initially uniform flow into the region of action electromagnetic forces, gives rise to intensive rotating flow, which stirs the original flow. At this point the flow completely loses its prehistory, maintaining only the flow rate. In this sense, the events that happen in the flow in front of the inductor are not critical. At the outlet boundary, the pressure is set to zero. The large eddy simulation (LES) model of Smagorinsky variant is used to describe the turbulence (constant $C_S = 0.1$ because the flow is bounded by the wall).

When selecting a constant, we relied on the experience of working with LES models of turbulence [26]. Since the problem deals with studying the integrity of the vortex as it moves downstream, we need a model that could best resolve the pulsations [27].

The calculations are carried out in a dimensional formulation without considering the channel walls. The magnetic fields rotating in opposite directions were generated by inductors 1 and 2 (Fig. 1), whose parameters are described in Ref. [8]. The length of cylindrical cell 3 (Fig. 1) is $L = 1\,\mathrm{m}$, the diameter $D = 2R = 0.1\,\mathrm{m}$. The distance between the magnetic field inductors is $M = 0.1\,\mathrm{m}$, the distance from the channel inlet to the plane between the inductors is $H = 0.2\,\mathrm{m}$. Each inductor consists of six windings, which are powered by the alternating current of frequency $f = 50\,\mathrm{Hz}$ with the phase difference $\pi/3$. For the problem under consideration, the depth of field penetration into the metal is 0.029 m, or $0.58 \cdot R$. The inductors produce a magnetic field of inductance B_0 in the cell. The duration of the action of electromagnetic forces is $\Delta t = 2\,\mathrm{s}$, and the time, at which they are switched on, is $t_1 = 3\,\mathrm{s}$. The following parameters were used for the liquid metal: density $\rho = 912.2\,\mathrm{kg/m^3}$, electrical conductivity $\sigma = 8.3$ MSm/m, kinematic viscosity $\nu = 0.55 \times 10^{-6}\,\mathrm{m^2/s}$.

The Taylor number (10) is used to estimate the parameters of electromagnetic forces and RMF and two Reynolds numbers are used to estimate the hydrodynamic processes

$$\mathrm{Ta} = \frac{\sigma 2\pi f B_0^2 R^4}{2\rho\nu^2}. \tag{10}$$

The first $\mathrm{Re}_T = V_T R/\nu$ defines the intensity of the axial flow that occurs in the absence of RMFs. Re_T is the input parameter, which varied in the range from 0 to 1.8×10^5. The second one $\mathrm{Re}_0 = V_0 R/\nu$ specifies the intensity of flow, which occurs in the absence of a given axial flow, i.e., at $V_T = 0$ and rotates with characteristic velocity V_0. For different Taylor numbers, Re_0 was from 0.5×10^5 to 1.8×10^5. These dimensionless parameters are given to generalize the results. And the third one, $\mathrm{Re}_A = V_A R/\nu$, characterizes the resulting azimuthal velocity ranging from 5×10^3 to 8×10^4.

The EMAG and FLUENT packages of the ANSYS software were used to carry out calculations. All calculations were performed using multiprocessor technology. Electromagnetic forces were specified through the user defined function interface. To generate a structured mesh and provide a satisfactory resolution of the calculations at the cylinder boundaries, the computational domain was divided into several subdomains. The computational domain of the hydrodynamic problem consists of more than 8×10^5 finite volumes. The average size of one element was $h = 3 \times 10^{-3}$ m, and the time step was $\tau = 0.01$ s. The Courant number $\tau \cdot u/h$ used in the numerical simulation did not exceed 1, where u is the characteristic velocity. This ensured the fulfillment of the stability condition for the numerical solution. The mathematical model for calculating the electromagnetic and hydrodynamic processes was verified using the experimental results obtained and described in Refs. [8,28,29].

III. RESULTS

The present study was based on multivariate calculations were performed in which the intensities of the azimuthal and axial velocity components, characterised by the quantities Re_0 and Re_T were varied. Calculations have shown that the most marked change in velocity occurs near the channel wall. Spatial and temporal diagrams for the profile of the V_y velocity component were plotted to explain the observed processes. In the diagram, the abscissa axis shows time, while the ordinate axis represents the coordinate along the channel on line 5 shown in Fig. 1. The value of the V_y component of the azimuthal rotation velocity is marked with color. The diagram allows us to describe the evolution of such a velocity profile. Figure 2 shows examples of several diagrams for different Re_T and fixed value of Ta. For $\mathrm{Re}_T = 0$ only, the RMF source is placed in the center of the channel where through flow is absent. In this case, after switching the electromagnetic forces, a pair of vortices is generated and their twisting is realized in opposite directions, which is an evident outcome Fig. 2(a). In the case of a weak transit flow, after the forces are switched on, the vortices spin up and begin to interact with each other Fig. 2(b). The first vortex V_1 (Fig. 1) runs over the second vortex V_2, the intensity of which decreases. After the forces are switched off, the pair of vortices is carried by the flow, which is accompanied with a rapidly decrease of their strength and distortion of their shape.

The most interesting effect occurs in the case of a strong transit flow. In this case, the boundaries of the vortex become more distinct and its shape becomes more perfect [Figs. 2(c) and 2(d)]. Figure 2(d) illustrates the case of the most localized solitary vortex, which is carried by the flow with almost unchanged structure. Similar results are demonstrated by the time dependencies of the V_y velocity component (Fig. 3), plotted for two different points on the same line 5 (Fig. 1). In the case of weak transit flow [Figs. 3(a) and 3(b)], the vortex migration can be traced from the evolution curves, which by themselves are essentially different. This demonstrates significant changes in the shape of the vortices. In the case of a strong transit flow, the vortex migration is clearly distinguishable [Figs. 3(c) and 3(d)]. The vortex boundaries are clearly defined on the signal itself, and the velocity V_y rapidly decreases to almost zero value after fast increasing.

In the case shown in Fig. 3(d), the localized solitary vortex is carried by the transit flow along the channel. Worthy of note is the fact that in this case the liquid metal outside the vortex does

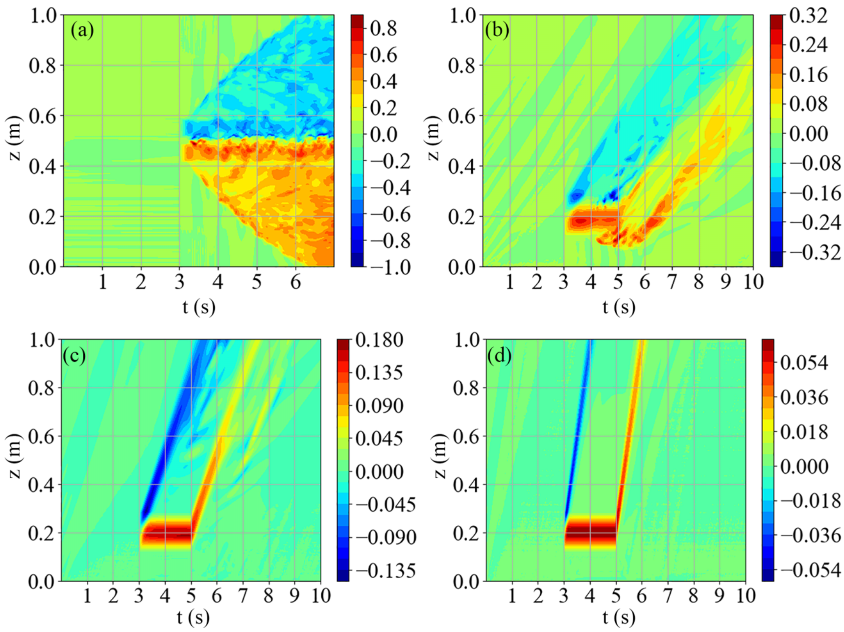

FIG. 2. Diagrams of velocity V_y profile evolution for the following values of axial transit velocity: (a) $V_T = 0\,\mathrm{m/s}$, (b) $V_T = 0.2\,\mathrm{m/s}$, (c) $V_T = 0.4\,\mathrm{m/s}$, (d) $V_T = 1\ \mathrm{m/s}$. Results are given for , $\mathrm{Ta} = 0.56 \times 10^5$.

not rotate in the channel, i.e., the velocity $V_y = 0$. For this case, the instantaneous fields of the V_y velocity component in cross section 4 (Fig. 1) for some moments of time are shown in Fig. 4. First, a pair of vortices V_1 and V_2 are formed, Fig. 4(a). Then, the second vortex V_2 is quickly carried away by the flow, Fig. 4(b), so that instead of a pair of vortices, there remains only one vortex V_1 [Fig. 4(c)], which shifts to the region between the RMF sources. After the electromagnetic forces are switched off, the vortex V_1 is also carried away by the transit flow, Fig. 4(d).

In the case of strong through flow the duration of the action of electromagnetic force Δt does not affect the behavior of the system. Figure 5(a) shows, as an example, the diagram for the velocity profile V_y under a long-time action of forces up to $\Delta t = 6\,\mathrm{s}$ for the same value of Re_T as was used in Fig. 2(d). The vortex shape did not change with increasing time of the force action, while the maximum and minimum values of velocity V_y remained unchanged. In turn, the velocity of the vortex depends on the intensity of electromagnetic forces, which are characterized by the Taylor number Ta (10). The intensity of azimuthal vortex flow in the absence of axial flow ($\mathrm{Re}_T = 0$) is characterized by the Reynolds number Re_0. The results of calculation show that the dependence of the vortex intensity on closely located sources of electromagnetic forces is close to a linear relationship, Fig. 5(b), in the investigated range of parameters, as in the work [9]. In this case, the dependence of the azimuthal velocity in the transit flow, characterized by Re_A, on the axial flow velocity is close to an inversely proportional relationship, Fig. 6(a). The axial velocity reaches its lowest value at the highest azimuthal velocity. This can be explained both by the strong interaction of the first V_1 and the second V_2 vortices and the growth of the turbulence influence. Turbulence provides mixing of the entire flow, including the azimuthal vortex, leading to a decrease of its intensity.

The threshold value of the parameters at which a solitary vortex is formed can be estimated as follows. Figure 6(b) shows the deviation of the velocity V_y from zero in the region far from the source of RMF as a function of the ratio $\mathrm{Re}_T/\mathrm{Re}_0$. In the regimes $\mathrm{Re}_T < \mathrm{Re}_0$, a significant deviation of the velocity V_y from zero is observed. In this case, the rotation spreads over the whole space of the channel with liquid metal, and the signal is obtained in a diffuse form, Figs. 3(a) and 3(b). For

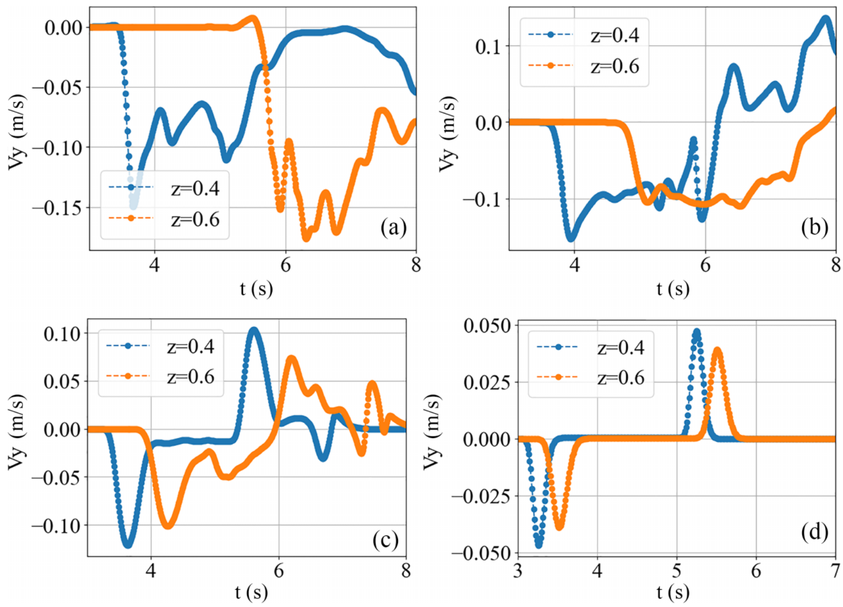

FIG. 3. The velocity V_y component vs time for the following values of axial transit velocity in a couple points placed on the line 5 (Fig. 1): (a) $V_T = 0\,\mathrm{m/s}$, (b) $V_T = 0.2\,\mathrm{m/s}$, (c) $V_T = 0.4$ m/s, (d) $V_T = 1$ m/s. Results are given for $\mathrm{Ta} = 0.56 \times 10^5$.

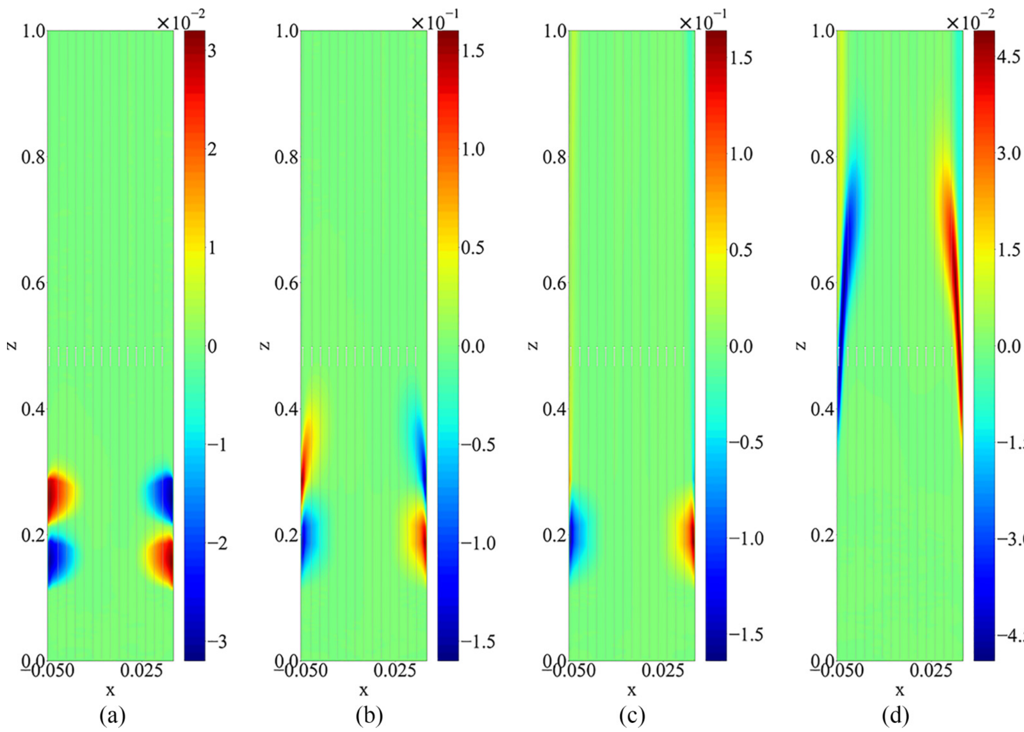

FIG. 4. Snapshots of V_y component of velocity filed in axial plane 4 (Fig. 1) for the following time: (a) 3 s, (b) 3.2 s, (c) 4.5 s, (d) 5.6 s.

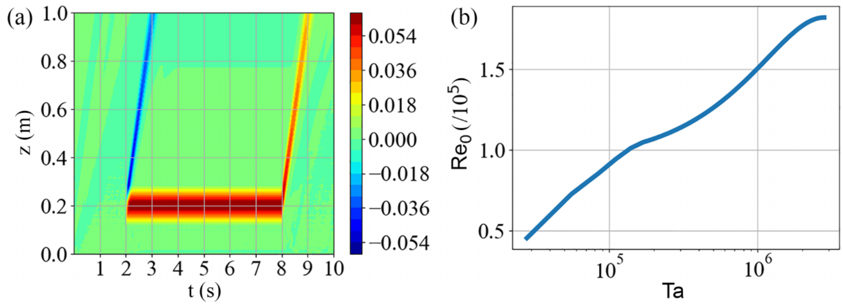

FIG. 5. (a) diagram of velocity V_y profile evolution during longer period Δt for $V_T = 1$ m/s. (b) Reynolds number Re_0 vs Tailor number Ta.

$Re_T \geqslant Re_0$ at some distance away from the sources of RMFs the rotation of liquid metal in the intensive transit flow is almost absent, Figs. 3(c) and 3(d). Thus, the transition from one flow regime to another occurs when Re_T and Re_0 are almost equal.

Correlation analysis of signals V_y at given pairs of points along the allowed us to estimate the degree of vortex flow intensity loss. The correlation function for signals at two points $V_y(0, y_A, z_1, t)$ and $V_y(0, y_A, z_2, t)$ is $C(\tau) = \int_0^T V_y(0, y_A, z_1, t) V_y(0, y_A, z_2, t + \tau)\, dt$. Here y_A determines the position of segment 5 in Fig. 1. The function can also be used to define the flow velocity as the ratio of the distance between points $\delta z = z_2 - z_1$ and time τ_A, determined by the maximum of the correlation function [30]. Calculations have shown that at low velocities of axial flow ($Re_A = 0.2$, $Re_A = 0.4$), the vortex quickly decays during migration along the channel. This leads to a blurring of the shape of the vortex. Correlation analysis shows a significant decrease in the maximum of the correlation function even at small distances δz [Fig. 7(a), blue and orange colors]. Thus, the solitary vortex does not keep its shape in weak transit flow.

For a strong transit flow, the correlation function is close to unity at a distance δz up to half a meter [Fig. 7(a), red and green colors]. The magnitude of the correlation function also exceeds the value of 0.9 and for slower flows ($Re_A = 0.6$, $Re_A = 0.8$) in a narrow range of values $\delta z < 0.2$ m. Thus, in this configuration, the solitary vortex in a strong through flow retains its perfect shape at a distance up to the center of the channel. The dependence of the correlation coefficient value on the Re_T/Re_A ratio reaches saturation at $Re_T > Re_A$, Fig. 7(b). Figures 6(a) and 7(b) show the regions of high, moderate, and low correlation in color. These regions actually determine the parameters that influence the formation of a solitary vortex in a strong through flow.

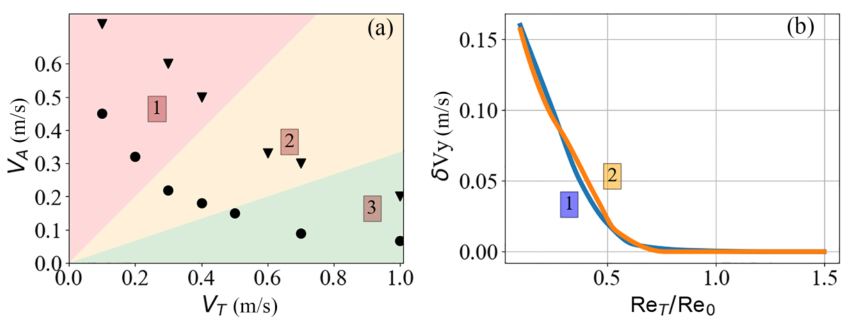

FIG. 6. (a) The maximum of velocity V_y component V_A vs axial transit velocity V_T. (b) Difference δV_A between the V_A velocity and zero in the region of the channel placed outside the region of RMFs acting: $1 - \mathrm{Ta} = 0.56 \times 10^5$; $2 - \mathrm{Ta} = 1.68 \times 10^5$.

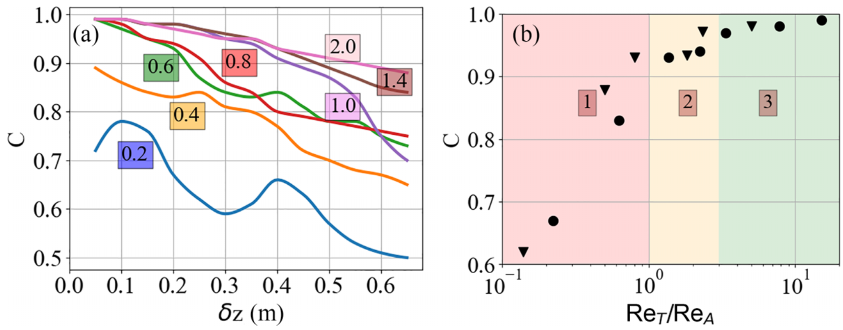

FIG. 7. (a) Maximum of correlation function vs distance between couple points placed on the line 5 (Fig. 1) for a several values of $\mathrm{Re}_T/\mathrm{Re}_0$ relation which indicated by numbers, $\mathrm{Ta} = 0.56 \times 10^5$. (b) Maximum of correlation function vs $\mathrm{Re}_T/\mathrm{Re}_A$ relation, dots for $\mathrm{Ta} = 0.56 \times 10^5$, triangles for $\mathrm{Ta} = 1.68 \times 10^5$. Here and on the Fig. 6(a) colored regions corresponds to the correlation function values: 1: smaller than 0.9; 2: smaller than 0.95; 3: larger than 0.95.

IV. SUMMARY

The main finding of the study is the discovery of a flow regime, which provides the existence of a solitary vortex in a transit flow. The axis of rotation of the vortex is aligned with the axis of the cylindrical channel. This vortex is localized in the direction of the axis, i.e. has sharp boundaries. The important thing is that initially two vortices are created in the channel, and eventually only one vortex is left. This process can only be implemented in a noncontact manner using the electromagnetic forces generated by inductors of rotating magnetic fields.

The study performed reveals the region of parameters providing the formation of a solitary rotating vortex. For different ratios of azimuthal and axial flow intensities, the flow pattern is as follows. The electromagnetic forces initially generate two vortices rotating in different directions in the channel at any values of axial velocity.

At low intensity of the axial flow, the rotating vortex made by RMFs propagates a considerable distance along the channel Fig. 8(a). Simultaneously, both vortices are carried by a slow axial through flow. Furthermore, the intensity of the second downstream vortex V_2 slightly decreases due to the nonlinear interaction with the first overrunning vortex V_1. The shape of the vortices becomes washed out as they migrate downstream. The boundary between these vortices is always blurred.

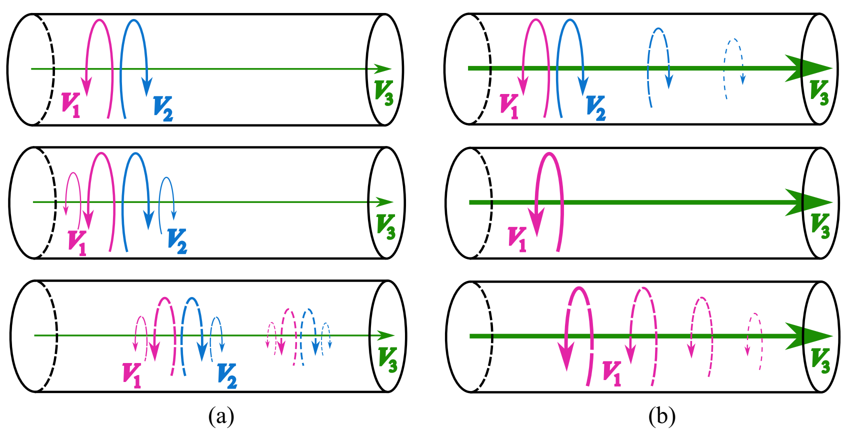

FIG. 8. Schematics of the rotating flow evolution stages (from top to bottom) for (a) weak and (b) strong axial transit flow V_T.

This is confirmed by the fact that the correlation analysis of the azimuthal velocity gives a low value of the correlation function between two points along the channel Fig. 7(b).

At high intensity of the axial flow, the process changes significantly. The second vortex V_2 is completely suppressed by the first vortex Fig. 8(b). The vortex V_1 propagates along the flow within a distance to the boundary between the RMFs. After completion of the transient period, it exists in a stationary state during the time of the action of electromagnetic forces Δt. The intensity of the azimuthal velocity becomes smaller than in the previous case due to the nonlinear interaction between the flows. The vortex V_1 is localized in the space M between the regions of generation of counter-rotating vortices by electromagnetic forces Fig. 5(a). The rotating vortex has clear-cut boundaries. In the flow regions before and after the vortex generation, the vorticity is close to zero. After the switch-off the electromagnetic forces, the vortex V_2 is carried by the axial flow along the channel.

At intermediate values of the axial flow, the vortex shape is less perfect, and in the channel region behind the vortex there is a residual rotation of the fluid. It is possible to determine a threshold value of axial velocity, at which a solitary vortex is formed. When this value is exceeded, the velocity of the residual rotation of the fluid becomes close to zero Fig. 6(b). The calculation showed that the threshold value is reached near the equality of Reynolds numbers $\mathrm{Re}_0 \sim \mathrm{Re}_T$.

The degree of the solitary vortex formation is determined by the correlation analysis of its transport along the flow after the switch-off of the forces. A high level of correlation between the azimuthal velocity signals at points along the channel, Fig. 7(a), indicates a good localization of the vortex. In this case the value of the axial velocity evaluated by correlation analysis is close to the actual value of the through flow velocity. This confirms that the vortex transport is similar to passive impurity transport. In this case, the vortex acts as a solitary Lagrangian marker frozen in the flow.

Such behavior of the system is not observed over the entire range of parameters. At high axial velocity, a high level of turbulence leads to a disturbance of the perfect solitary vortex shape. In our further research we plan to find how the imbalance of the electromagnetic forces, as well as the variation of their spatial parameters influence the process.

Thus, the measurement of the liquid-metal velocity can be implemented in the following way. Using the proposed technique a localized solitary vortex with intense azimuthal component is created. With an appropriate selection of parameters, after switching out the forces, the structure of the vortex transported by the flow remains almost unchanged. To measure the flow velocity, it is necessary to place two sensors on the outer surface of the channel at a distance of L_p from each other. The sensors are brought into action as soon as the vortex passes by. Knowing the time interval between the activations of two sensors Δt_p, we can determine the velocity of the solitary vortex $V = L_p/\Delta t_p$, and hence of the flow [21]. The measurement can be made with the induction sensor described, for example, in Ref. [31]. The main advantage of the technique is that it does not require calibration. Thus, the practical usefulness of the technique lies in the possibility of its application for noncontact measurement of liquid metal velocity. Perhaps it will contribute to the stability of the solitary vortex shape and extend the range of parameters ensuring its perfect form.

ACKNOWLEDGMENT

The work was carried out as part of a major scientific project funded by the Ministry of Science and Higher Education of the Russian Federation (Agreement No. 075-15-2024-535 dated 23 April 2024).

DATA AVAILABILITY

The data that support the findings of this article are not publicly available upon publication because it is not technically feasible and/or the cost of preparing, depositing, and hosting the data would be prohibitive within the terms of this research project. The data are available from the authors upon reasonable request.

[1] P. A. Davidson, *An introduction to Magnetohydrodynamics* (Cambridge University Press, London, 2001).
[2] François rincon, dynamo theories, J. Plasma Phys. **85**, 205850401 (2019).
[3] A. Gailitis, O. Lielausis, S. Dement'ev, E. Platacis, A. Cifersons, G. Gerbeth, T. Gundrum, F. Stefani, M. Christen, H. Hänel, and G. Will, Detection of a flow induced magnetic field eigenmode in the Riga dynamo facility, Phys. Rev. Lett. **84**, 4365 (2000).
[4] K. Steglitz and U. Mueller, Experimental demonstration of a homogeneous two-scale dynamo, Phys. Fluids **13**, 561 (2001).
[5] H. K. Moffatt, Electromagnetic stirring, Phys. Fluids **3**, 1336 (1991).
[6] Yu Gelfgat and J. Priede, Mhd flows in a rotating magnetic field (a review), Magnetohydrodynamics **31**, 214 (1995).
[7] I. Kolesnichenko, A. Pavlinov, E. Golbraikh, P. Frick, A. Kapusta, and B. Mikhailovich, The study of turbulence in MHD flow generated by rotating and traveling magnetic fields, Exp. Fluids **56**, 88 (2015).
[8] I. Kolesnichenko and R. Okatev, Equalisation the toroidal and poloidal kinetic energies of liquid metal stirring flow, Eur. Phys. J. Plus **139**, 846 (2024).
[9] V. Ozenykh, G. Losev, E. Golbraikh, and I. Kolesnichenko, Initial stage of formation of vortex flow in an inductor with counter-rotating magnetic fields, Comput. Continuum Mech. **16**, 493 (2023).
[10] J. A. Shercliff, *Theory of Electromagnetic Flow Measurement* (Cambridge University Press, Cambridge, 1962).
[11] T. Schulenberg and R. Stieglitz, Flow measurement techniques in heavy liquid metals, Nucl. Eng. Des. **240**, 2077 (2010).
[12] R. Khalilov, I. Kolesnichenko, A. Mamykin, and A. Pavlinov, A combined liquid sodium flow measurement system, Magnetohydrodynamics, **52**, 53 (2016).
[13] S. Eckert, D. Buchenau, G. Gerbeth, F. Stefani, and F. Weiss, Some recent developments in the field of measuring techniques and instrumentation for liquid metal flows, J. Nucl. Sci. Technol. **48**, 490 (2011).
[14] V. Sharma, G. Vijaya Kumar, S. K. Dash, B. K. Nashine, and K. K. Rajan, Modeling of permanent magnet flowmeter for voltage signal estimation and its experimental verification, Flow Meas. Instrum. **28**, 22 (2012).
[15] A. Pavlinov, R. Khalilov, A. Mamykin, and I. Kolesnichenko, Electromagnetic flowmeter for wide-temperature range intensive liquid metal flows, IOP Conf. Series: Mater. Sci. Eng. **581**, 012011 (2019).
[16] S. Poornapushpakala, C. Gomathy, J. I. Sylvia, and B. Babu, Design, development and performance testing of fast response electronics for eddy current flowmeter in monitoring sodium flow, Flow Meas. Instrum. **38**, 98 (2014).
[17] J. Forbriger and F. Stefani, Transient eddy current flow metering, Meas. Sci. Technol. **26**, 105303 (2015).
[18] A. Pavlinov, R. Khalilov, A. Mamikyn, and I. Kolesnichenko, Eddy current flowmeter for sodium flow, IOP Conf. Ser.: Mater. Sci. Eng. **208**, 012031 (2017).
[19] A. Thess, E. Votyakov, and Y. Kolesnikov, Lorentz force velocimetry, Phys. Rev. Lett. **96**, 164501 (2006).
[20] J. Priede, D. Buchenau, and G. Gerbeth, Force-free and contactless sensor for electromagnetic flowrate measurements, Magnetohydrodynamics **45**, 451 (2009).
[21] I. Belyaev, N. Razuvanov, V. Sviridov, and V. Zagorsky, Temperature correlation velocimetry technique in liquid metals, Flow Meas. Instrum. **55**, 37 (2017).
[22] E. V. Votyakov and S. C. Kassinos, On the analogy between streamlined magnetic and solid obstacles, Phys. Fluids **21**, 097102 (2009).
[23] I. Kolesnichenko, A. Mamykin, E. Golbraikh, and A. Pavlinov, Temperature correlation method application to the problem of measuring the flow rate of liquid sodium, Magnetohydrodynamics **57**, 547 (2021).
[24] O. Zikanov, I. Belyaev, Y. Listratov, P. Frick, N. Razuvanov, and V. Sviridov, Mixed convection in pipe and duct flows with strong magnetic fields, Appl. Mech. Rev. **73**, 010801 (2021).
[25] G. G. Branover and A. B. Tsinober, *Magnetohydrodynamics of Incompressible Media* [in Russian], (Nauka, Moscow, 1970).
[26] L. Zwirner, R. Khalilov, I. Kolesnichenko, A. Mamykin, A. Pavlinov, S. Mandrykin, A. Shestakov, A. Teimurazov, P. Frick, and O. Shishkina, The influence of the inclination angle on the heat transport and large-scale circulation in liquid metal convection, J. Fluid Mech. **884**, A18 (2020).

[27] A. Teimurazov and P. Frick, Thermal convection of liquid metal in a long inclined cylinder, Phys. Rev. Fluids **2**, 113501 (2017).

[28] I. Kolesnichenko, P. Frick, V. Eltishchev, S. Mandrykin, and F. Stefani, Evolution of a strong electrovortex flow in a closed cell, Phys. Rev. Fluids **5**, 123703 (2020).

[29] P. Frick, S. Mandrykin, V. Eltishchev, and I. Kolesnichenko, Electro-vortex dynamics in a cylindrical cell under axial magnetic field, J. Fluid Mech. **949**, A20 (2022).

[30] R. Khalilov, I. Kolesnichenko, A. Pavlinov, A. Mamykin, A. Shestakov, and P. Frick, Thermal convection of liquid sodium in inclined cylinders, Phys. Rev. Fluids **3**, 043503 (2018).

[31] S. Miralles, G. Verhille, N. Plihon, and J.-F. Pinton, The magnetic-distortion probe: Velocimetry in conducting fluids, Rev. Sci. Instrum. **82**, 095112 (2011).